Cellular burning in lean premixed turbulent hydrogen-air flames: coupling experimental and computational analysis at the laboratory scale

M. S. Day[1], **J. B. Bell**[1], **R. K. Cheng**[2], **S. Tachibana**3, **V. E. Beckner**[1], **M. J. Lijewski**[1]

[1]Center for Computational Science and Engineering, Lawrence Berkeley National Laboratory, Berkeley, CA, 94720
[2]Environmental Energy Technologies Division, Lawrence Berkeley National Laboratory, Berkeley, CA, 94720
[3]Environmental Energy Technologies Division, Lawrence Berkeley National Laboratory, Berkeley, CA, 94720, currently at Japan Aerospace Exploration Agency, Tokyo, Japan

E-mail: `msday@lbl.gov`

Abstract. One strategy for reducing US dependence on petroleum is to develop new combustion technologies for burning the fuel-lean mixtures of hydrogen or hydrogen-rich syngas fuels obtained from the gasification of coal and biomass. Fuel-flexible combustion systems based on lean premixed combustion have the potential for dramatically reducing pollutant emissions in transportation systems, heat and stationary power generation. However, lean premixed flames are highly susceptible to fluid-dynamical combustion instabilities making robust and reliable systems difficult to design. Low swirl burners are emerging as an important technology for meeting design requirements in terms of both reliability and emissions for next generation combustion devices. In this paper, we present simulations of a lean, premixed hydrogen flame stabilized on a laboratory-scale low swirl burner. The simulations use detailed chemistry and transport without incorporating explicit models for turbulence or turbulence/chemistry interaction. Here we discuss the overall structure of the flame and compare with experimental data. We also use the simulation data to elucidate the characteristics of the turbulent flame interaction and how this impacts the analysis of experimental measurements.

1. Introduction

Within the combustion industry there is considerable interest in developing fuel-flexible burners that can be used to stabilize lean premixed flames in a stationary turbine designed for power generation. Low-swirl burner technology, originally introduced by Bedat and Cheng [1] as tool for studying the fundamental properties of lean, premixed turbulent flames, has the potential for meeting this need. Burners based on modifications of the original design have been used by a number of research groups [2–5], and have the potential for use in the design of next-generation, lean premixed combustion systems, including those burning lean hydrogen at both at atmospheric and elevated pressures [6].

The low-swirl burner concept is extremely simple: premixed fuel exits a pipe after passing through a turbulence generation plate and an annular set of curved vanes. The vanes impart a swirl component to the flow over a narrow layer near the pipe

wall, and a detached premixed flame anchors in the diverging flow above the pipe exit. Turbulence in fuel stream wrinkles the flame, which enhances the overall rate of combustion in the device; the flames stabilize where the mean burning speed matches the axial flow velocity. Analysis of experimental velocity measurements for both lean hydrogen-air and methane-air mixtures shows that the mean burning speed of the low-swirl flames is proportional to the intensity of turbulence in the approach flow to the flame [6, 7], and that effective enhancement of the burning speed can exceed a factor of 50 or more. However, because the burner supports ultra-lean mixtures while also lacking a significant post-flame flow recirculation, nitrogen-based emissions are extremely low.

Figure 1: (a) Low-swirl nozzle, showing vanes and turbulence generation plate. (b) typical turbulent low-swirl methane flame stabilized in divergent flow above the low-swirl nozzle.

Continued development of these types of burners, particularly for alternative fuels, depends on improving our understanding of basic flame structure, stabilization mechanisms, emissions and response to changes in fuel. Numerical modeling has the potential to address some of these issues, but simulation of these types of burners has proven to be difficult because of the large range of spatial and temporal scales in the system; the bulk of the analysis to date has been experimental.

As noted in Bell et al. [8], the detailed structure of lean premixed flames becomes particularly important and difficult to simulate when burning hydrogen. Lean hydrogen-air flames burn in cellular structures—localized regions of intense burning, separated by regions of local extinction. In this regime, the flame surface is broken into discontinuous segments. This type of structure introduces severe difficulties in applying standard turbulence/chemistry interaction models, which are based on the presence of a highly wrinkled but continuous flame surface that propagates locally as an idealized laminar flame structure. The cellular burning patterns additionally make the analysis of experimental data problematic, and can lead to significant inaccuracies or misinterpretations. Analysis in Day et al.[9] examines the structure of lean premixed hydrogen flames in an multi-dimensional, time-dependent (but idealized) setting in some detail. It was found that turbulent fluctuations tend to disrupt the spontaneous development and evolution of the cellular burning structures. With increasing fluctuation instensity, the cells became larger, while the burning intensity, even in locally flat regions is elevated on average by factors of 3 or more. In the absence of a suitably general model for the turbulent combustion of lean hydrogen-air mixtures, numerical simulations must incorporate sufficient detail in the chemical kinetics, differential species transport and turbulent fluid dynamics to capture all the important couplings in these flows.

In this paper, we focus on detailed numerical simulation of a laboratory-scale lean hydrogen flame that is stabilized on a low-swirl burner. As in our previous work, the simulation is performed with detailed chemistry and transport without explicit turbulence models. The case considered here is at a relatively high turbulence intensity. We use the low-swirl burner configuration presented in [2] that is under investigation by several groups internationally using matched nozzle hardware. This particular configuration is designed specifically to support validations with computer simulation.
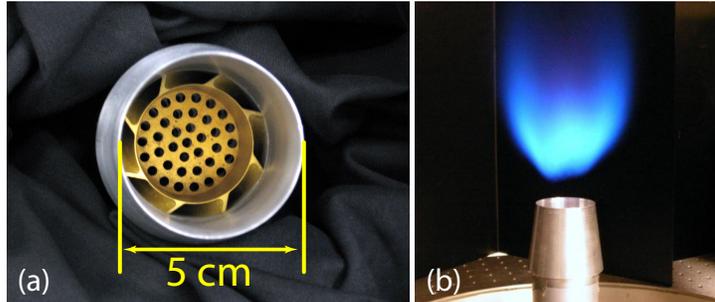
2. Numerical methodology

The simulations presented here are based on a low Mach number formulation [10] of the reacting Navier-Stokes equations. The methodology treats the fluid as a mixture of perfect gases. We use a mixture-averaged model for differential species diffusion, which is critical to capturing the thermodiffusive behavior of lean hydrogen flames (see [11] for a complete discussion of this approximation). We ignore Soret, Dufour and radiative transport processes. A lean hydrogen-air inlet fuel mixture (ϕ=0.37) was modeled with the hydrogen sub-mechanism of GRI-Mech 2.11; the transport coefficients and thermodynamic relationships are obtained from EGLib [12].

The basic finite-volume numerical discretization [13] combines a symmetric operator-split treatment of chemistry and transport with a density-weighted approximate projection method to impose the evolution constraint. The resulting integration proceeds on the time scale of the relatively slow advective transport. Faster diffusion and chemistry processes are treated implicitly in time. This integration scheme is embedded in an adaptive mesh refinement algorithm based on a hierarchical system of rectangular grid patches. The data and work are apportioned over a parallel computing system using a coarse-grained load distribution strategy [14]. The complete integration algorithm is second-order accurate in space and time, and discretely conserves species mass and enthalpy.

3. Computational Setup

There are two possible approaches for how to treat the nozzle in a simulation of this sort. One possiblility is to include the flow in the nozzle directly as part of the simulation; the alternative is to use measured data to prescribe the flow at the exit to the nozzle. In a series of studies, Nogenmyr et al. [4, 15, 16], considered both options in the context of LES simulations of lean methane-air mixtures. Considerably better agreement was found between simulated and measured profiles when the flow inside the nozzle was included. In particular, the simulations correctly predicted large-scale structures emanating in their configuration from the swirl vanes inside the nozzle, and these structures ultimately played a key role in stabilizing their flame. The measured and computed flows exiting the nozzle additionally exhibited a pronounced imprint of the swirl vane structure. Mean flow rates varied by as much as 30% azimuthally in the swirling-flow region, depending on whether the measurement plane was directly above a vane or a gap. A larger scale additional azimuthal variabilities of up to 20% were observed, and attributed to basic nonuniformities in the experimental setup. These nonuniformities led to an observed global shifting of the flame from the device center.

Recent modifications to the basic low-swirl nozzle design include: airfoil-like tapering of the trailing edges of the vanes to avoid formation of the large downstream vortical structures, varying the number and length of swirl vanes and their tilt with respect to the mean flow to improve the azimuthal symmetry of the device, and adjusting the geometry and orientation of the perforated turbulence generation plates. While such details have had significant impact on the global flame shape and resulting mean flow fields, which are important from an engineering/ performance point of view, experimental evidence suggests that the local flame propagation, including the detailed interactions of the flame chemistry and fine scales of the turbulence, is largely independent of these adjustments. This independence holds particularly well in the core region of the flame inside of the swirl-induced turbulent shear layer, and where much of the fuel consumption (and emissions generation) occurs.

The simulations here incorporate an experimental characterization of the flow at the nozzle exit. Typical profiles for this purpose were provided by Petersson et al. [2], and are shown in Fig. 2 as a function of radius from the centerline of the fuel pipe. Outside the pipe, a 35 cm/s upward coflow of cold air is specified. These profiles were generated using data collected from a ϕ=0.62 methane-air flame at a mean fueling rate of 6 m/s. Stereo PIV data was collected in a set of vertical planes to infer the three components of the mean velocity field.
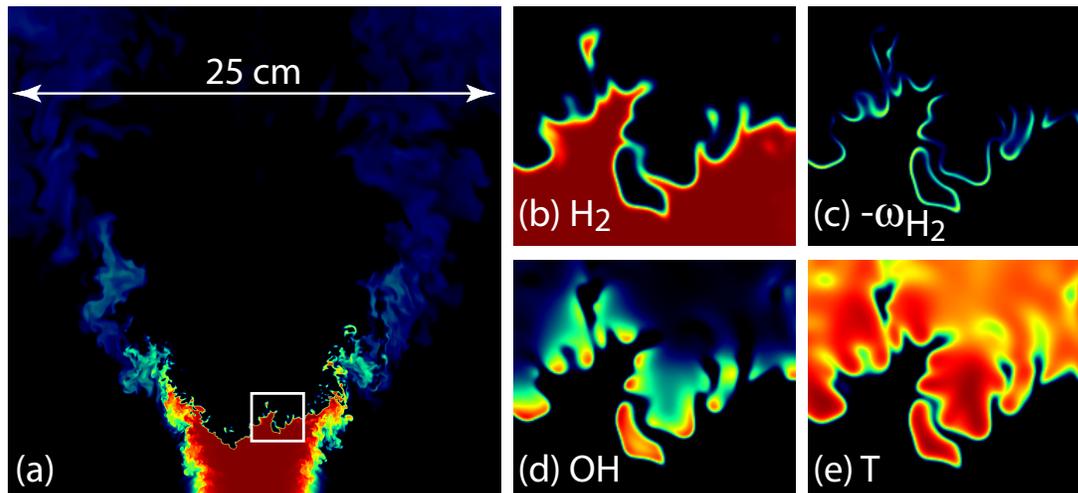
Figure 3: Typical slice from a snapshot in time of the computed flame solution. Panel represents a vertical slice centered on the symmetry axis of the nozzle. (a) The mole fraction of H_2 over a $(25\ cm)^2$. (b)-(e) Enlargements of the white-boxed region (approx. 2.5 cm wide) in (a). (b) H_2 mole fraction, (c) Destruction rate of H_2, (d) Mole fraction of OH, and (e) temperature. All scales are relative to the peak values over the domain at that instant.

These profiles were averaged azimuthally, and scaled by 250% to obtain a "ideal azimthally symmetric" laboratory-scale low-swirl nozzle operating at a mean mass flow rate of 15 m/s.

Turbulent fluctuations in the nozzle were prepared in an auxiliary simulation and added to the mean flows. An initially zero-mean velocity field, representative of flow through a perforated plate, is evolved until the measured integral length scale was 4 mm. A radial scaling factor was used to shape these synthetic fluctuations to the measured data.

The thermal thicknesses of this hydrogen-air flame is approximately 800 μm; the full half-width maximum of the fuel consumption rate is approximately 0.5 mm. The computational domain for the reacting flow simulations measures 25 cm^3. We implicitly assume that the boundaries of this box are sufficiently far from the flame as to not significantly affect its dynamics. The base mesh for the simulation is a uniform grid of 256^3 cells and uses 3 additional levels of factor-of-two dynamic grid refinement which track regions of high vorticity (turbulence) and reactivity (combustion/flame). The flame is contained entirely within the finest level, for an effective resolution of 2048^3. We run the simulations from an arbitrary initial condition until the flame is statistically stationary. In previous work, we demonstrated that this level of resolution is adequate to capture the detailed structure of the flame including the peak fuel consumption, the thermal field and major species.

Figure 2: Inlet velocity profiles at the exit plane of the swirl nozzle, adapted from experimental data [2].

4. Simulation Results

In Figure 3, we show a cross-section through the middle of the simulation that provides a picture of the overall structure of the flame. The swirl introduced in the outer portion of the injected mixture induces a flow divergence, and a negative gradient in vertical velocity.
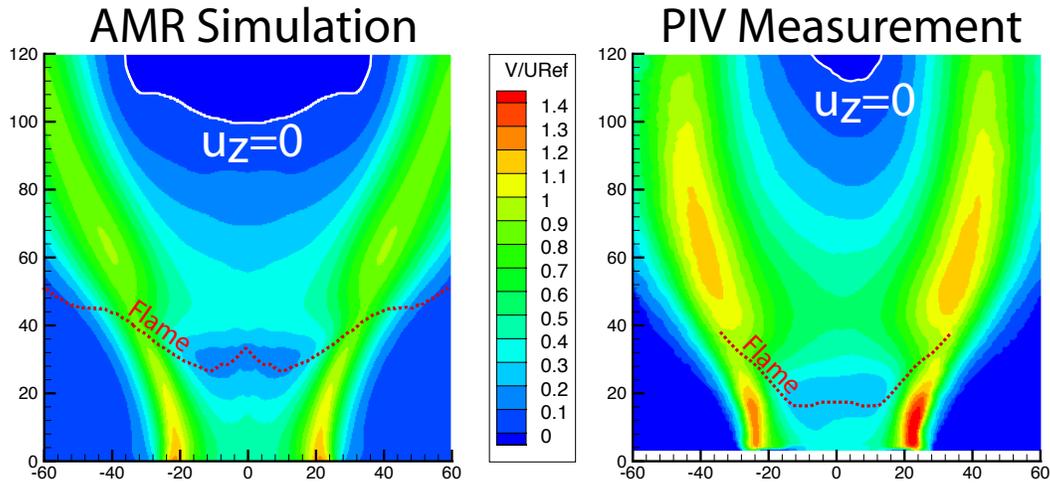
Figure 5: Comparison of the mean vertical velocity (scaled by the mean fueling rate) for the simulated ideal low-swirl nozzle, and a representative experimental profile. A number of key features are recovered in the simulations, including the weak recirculation approximately 10 cm downstream of the nozzle. The computed flame position sits somewhat downstream of the measured data, consistent with the simulation's higher mean velocity in the core.

The decreasing axial velocity provides a robust aerodynamic-based mechanism for flame stabilization. In the upper part of the simulation, one sees a low concentration of unburnt fuel (blue). This represents fuel that has been sufficiently diluted with air that it is below the flamability limit. Turbulent fluctuations from two primary sources interact with the flame (see Figure 4). Fluctuations introduced at the inlet boundary advect toward the flame, wrinkling the central core region. Also a swirl-generated shear layer forms on the outer edge of the burner nozzle, which leads to mixing of fuel and air on the sides of the burner.
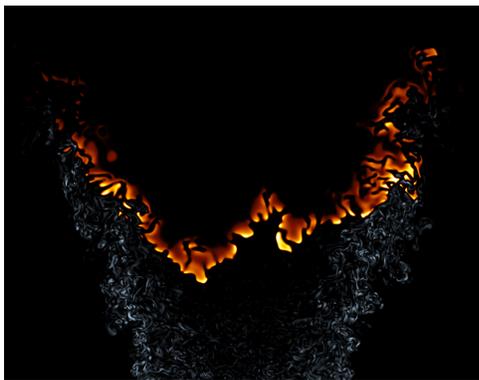
Figure 4: Composite image (cropped in near the flame/nozzle region) simultaneously shows the OH intensity (in orange) and the magnitude of vorticity (in grey). Turbulence approaches the flame from the core of the inlet nozzle at the lower domain boundary, and is generated by shear in the swirling flow region.

The idealized inlet profile we used has no experimental counterpart to date; the physical laboratory device exhibits considerable azimuthal variabilities due to the vane structure and location. Furthermore, additional analysis of experimental data suggests a Reynolds number dependence of the inflow at lower fueling rates from which the initial data from this simulation was taken. Nevertheless, Figure 5 compares the mean axial velocity profile taken from a low-swirl nozzle flame with identical fuel mixture, fueling flow rates and nozzle swirl number. Coloring in the two plots is identical. Obtaining converged statistics for the simulation is difficult because of the computational expense of long-time integrations. To reduce this requirement, we used azimuthal averages of the simulation data to compute mean profiles. This produces reasonable data for most of the domain but give poor statistics near the center of the burner. From the comparison, the experiment shows a significantly lower central velocity and somewhat higher velocity near the edge of the burner (20 mm) than the boundary data used for the simulation. The simulation predicts a higher flame location, which is consistent with the higher inflow velocity. (We note
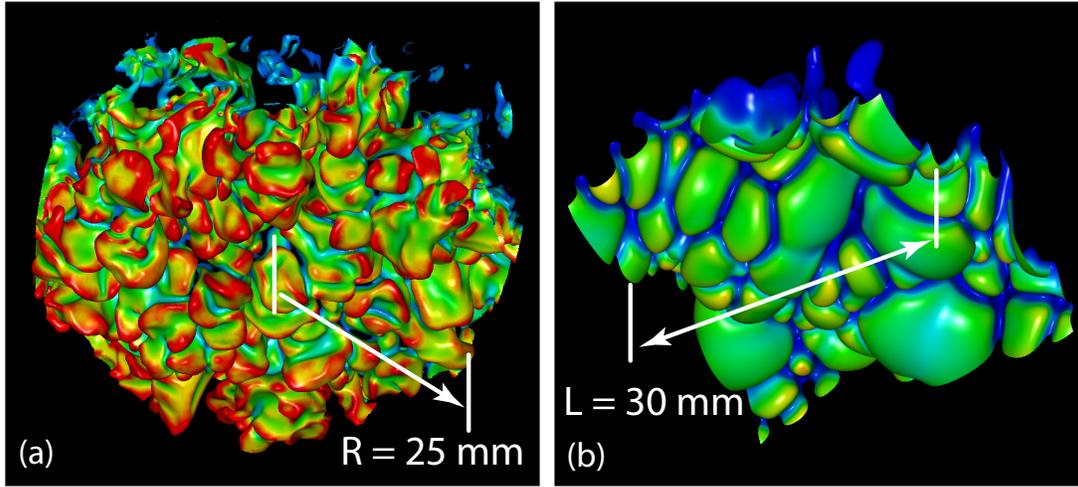
Figure 6: *Flame isotherm, T= 1144 K, colored by the local rate of H_2 consumption. (a) Low-swirl flame isotherm, conditioned on r < 25mm, z <8mm. (b) Representative isotherm of an idealized ϕ=0.37 H_2-air flame propagating freely in uniform flow.*

that the appearance of a raised flame location near the origin may well be an artifact of the lack of data in this region.) Nevertheless, the simulation is consistent with a low-swirl nozzle with somewhat different flow characteristics.

Although there are qualitative differences in the global structure of the flame, we can still compare the details of the local flame structure in the experiment and the simulation. Lean hydrogen-air flames are thermodiffusively unstable and burn in cellular structures; even in the absence of turbulence, the flame will not burn as a stable continuous interface. Here, the turbulent flow in the central core of the burner serves as additional source of wrinkling of the flame. In Figure 6, we show the T= 1144 K isotherm, colored by local fuel consumption in the core of the burner. For comparison, we also show the analogous image for a freely propagating hydrogen flame (taken from the study in [9]). Both images are based on the same color map, and the length scales are as indicated in the figure. Comparing these images, one can see that in the turbulent flame, there are finer structures than in the non-turbulent case. The turbulent flame shows more ridge-like structures compared to the freely propagating flame in which the features are more bulbous. Finally, the burning rate over most of the flame surface is considerably higher in the turbulent configuration, particularly where the flame is tightly folded.

One of the principal diagnostics used in the experiments is OH-PLIF (planar laser-induced fluorescence) based on imaging the flouresence of OH radicals excited by a tuned laser sheet. In Figure 7, we show a typical vertical slice of the OH concentration from the simulation alongside typical PLIF images from the experiment. Figure 7(a) shows the profile of OH over the $(25\text{ cm})^2$ slice, while Figures 7(b) and (d) show progressive enlargements of the data corresponding to the field of view of the typical OH-PLIF data shown in Figures 7(c) and (e). The experimental data are representative images taken from the low-swirl experiment. The figure show that the simulation captures features of these flames, with remarkably similar sizes, shapes and global structure. The simulation also captures the observed variability of the OH signal (brightness on the experimental images) along the flame surface. Previous work on turbulent hydrogen flames shows that the high diffusivity of H_2 can lead to local enrichment of the fuel mixture along the front. This local enrichment can lead to intensification of local burning, which leads to increased OH that can be seen experimentally as a brigher signal in the OH PLIF (and red regions in the simulation slice data).

From analysis of the simulation data, we can obtain a detailed characterization of the
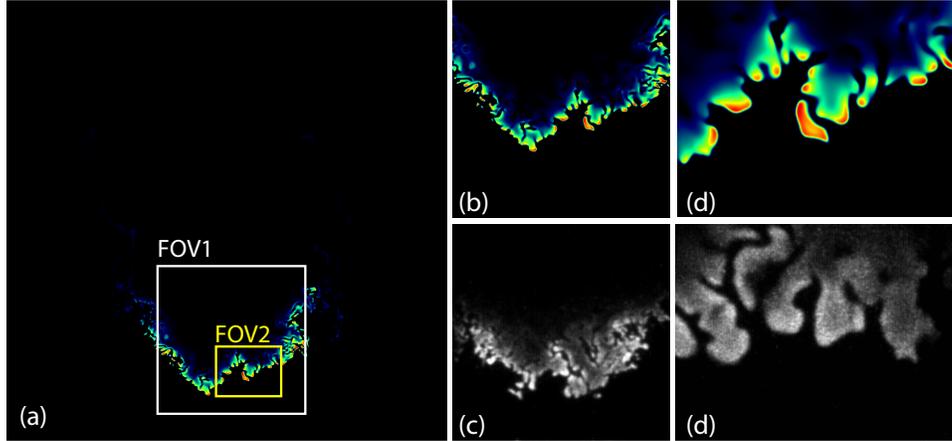
Figure 7: (a) Typical slice of OH concentration on vertical midplane from the simulation. Red indicates high relative values, and are correlated with the flame front. The white box ("FOV1") represents the field of view of OH-PLIF measurements from the representative low swirl experiment focused on the large-scale flame structure. The smaller yellow box ("FOV2") represents the experimental field-of-view OH-PLIF measurements focused more tightly on the local structure of the flame surface (width of FOV2 is approximately 26 mm). (b) Zoom of profile in (a) over FOV1, (c) typical experimental OH-PLIF image over FOV1, (d) Zoom of profile in (a) over FOV2, and (e) typical experimental OH-PLIF image over FOV2.

local flame structure that is not feasible from the experimental data. We begin with an examination of the fuel consumption rate. As with the OH-PLIF data, the fuel consumption shows considerable variability along the flame front. To quantify this behavior, we extract the T=1144 K surface (trimmed to r<5 cm, z<8 cm; outside this window, the isotherm is shredded by the swirl-induced shear layer). This temperature corresponds to the that of peak fuel consumption in the flat laminar flame at ϕ=0.37. We further trim the surface to exclude regions where the fuel consumption is less than half the laminar flame value. On the remaining sections of the flame isotherm, we can then evaluate mean and Gaussian curvatures (using approaches outlined in [9]). In Figure 8a and Figure 8b we show PDF's of of the two measures of curvature. We note that for the turbulent flame, the distribution of mean curvature is considerably broader and more symmetric than the non-turbulent flame. The Gaussian curvature is also more symmetric about zero. These observations indicate that turbulence serves to disrupt the bulbous structures characteristic of the freely propagating flame. The symmetric Gaussian curvature peaked near zero is a signature of the rib-like structures seen in Figure 6.

Figure 8: Distributions of mean and Gaussian curvatures of the flame isotherm (conditioned on r<5 cm, z<8 cm), scaled to the thermal thickness of the laminar H_2-air flame at ϕ=0.37.

To relate the local geometry to the local flame properties, we define a local consumption-based flame speed on the isotherm. For this construction we first define a local coordinate system on that surface as depicted in Figure 9. Associated with each triangle on the surface, we can then associate a prismatic region. We can
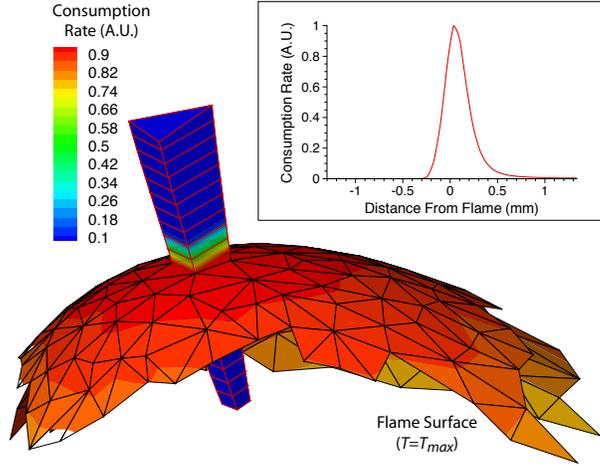
Figure 9: Prism-shaped volume, Ω, constructed using curves locally normal to the temperature isotherms (both the flame and Ω are colored by a typical profile of fuel consumption rate, ω_{H2}). The inset plot shows the variation of ω_{H2} normal to the flame surface. Ω discretizes the flame volume, and the integral curves of T that bound Ω define a set of local flame coordinates.
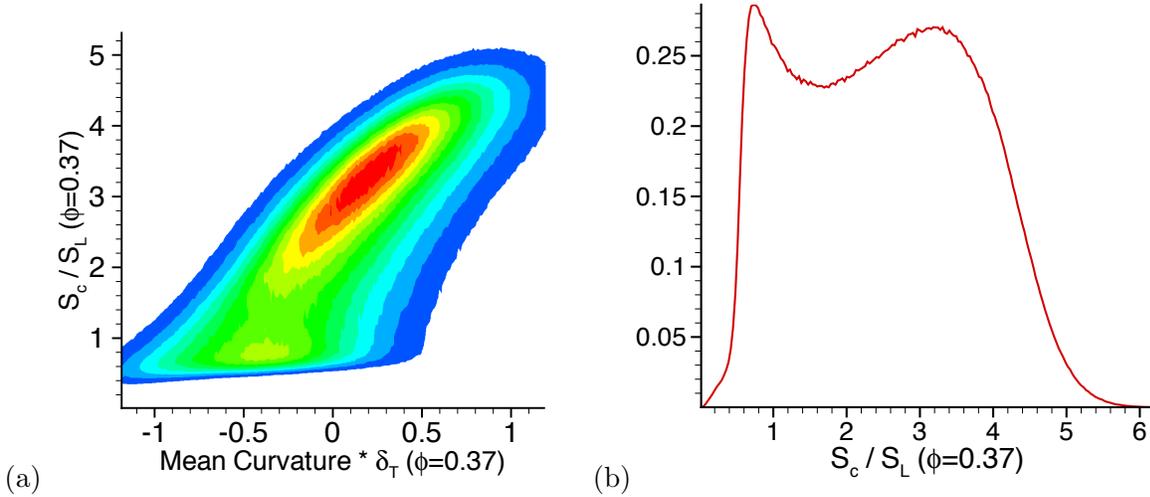
Figure 10: (a) Joint PDF of local consumption speed, s_c^ℓ, with mean curvature, (b) Distributions of s_c^ℓ over the entire conditioned flame surface. in both plots, the burning speed is normalized by the speed of the flat H_2-air flame at $\phi=0.37$.

then define a local consumption speed as

$$s_c^\ell = \frac{1}{A\left(\rho Y_{H_2}\right)_{\text{in}}} \int_\Omega \omega_{H_2} d\Omega \tag{1}$$

In Figure 10(a) we show a joint PDF of mean curvature and s_c^ℓ, normalized the laminar burning speed, s_L, of a flat steady hydrogen-air flame at $\phi=0.37$. This figure shows a strong correlation between local burning speed and curvature. Regions of intense burning correspond to regions of positive curvature (positive curvature corresponds to regions where the center of curvature is on the products side of the flame interface). Also note that the dominant behavior corresponds to local burning speeds that range from 2 to 4 times the laminar flame speed. Even at zero curvature, the most probable local burning speed is three times the laminar flame speed. As discussed in [9], this enhanced burning reflects local enrichment of the fuel resulting from

preferential diffusion of H_2 into burning regions. If we integrate out the curvature dependence, we can derive a PDF of local consumption speed along the flame front, shown in Figure 10(b). This PDF shows dual peaks, one corresponds to weak burning at less than the laminar flame speed and a second broader peak at about 3.3 s_l, again illustrating the structure of cellular structures.

Experimentally, it is not possible to directly measure fuel consumption. However, the similarities in the variation of fuel consumption rate and the OH concentation along the flame front suggest that there might be a correlation between them (see Figure 3). In Figure 11, we show a JPDF of s_c^ℓ versus the peak of OH mole fraction along the local coordinate normal to the flame surface. In the Figure, we have overlain the corresponding relationship for flat laminar flames at a range of equivalence ratios. The data serves to quantify the enrichment of the flame due to preferential diffusion mentioned earlier. In particular, the highest probability region in the JPDF corresponds to laminar flames burning in the range $\phi = 0.48$–0.50.

There is a clear and strong correlation between peak OH and local flame speed, which is somewhat steeper than the locus of laminar flames, although the variability is somewhat broader for lower flame speeds. Nevertheless, this correlation could be used to relate measured OH signal from PLIF to a local consumption-based flame speed [17]. However, to fully develop this type of diagnostic, one would need to account for the effects of quenching. In particular, one could compute the synthetic laser intensity as in [18, 19], using the simulation data to compute quenching

Figure 11: Joint PDF showing the strong correlation between local burning speed and the nearby peak values of the OH concentration.

and develop a correlation between local flame speed and synthetic OH intensity. Of course, the viability of this type of approach would assumes that image intensities can be measured with sufficient accuracy to interpret them quantitatively. It is worth noting that in this lean hydrogen-air mixture, the OH-PLIF signals will be low making making quantitative measurement challenging to obtain.

5. Discussion and Future Work

We have presented results from a detailed numerical simulation of a laboratory-scale low-swirl turbulent lean hydrogen flame. The simulation incorporated detailed chemistry and transport without explicit turbulence models. Mean velocities and flame positions were compared with a similar laboratory configuration, and many key salient features of the flame and flowfield were reproduced. The turbulent flame surface was found to be highly corrugated by the turbulence and shows considerable local variability in instantaenous fuel consumption rates. The local and global distribution of OH compared well with experiment, and was shown to correlate well with the local speed of flame propagation. Compared to a freely propagating idealized case, the local curvature of the flame surface shifts from predominantly positive (where the center of curvature is on the products side of the flame) to symmetrically distributed around zero, with a much broader distribution. The predominant shape of the burning cells also shifts dramatically from spherical to cylindrical.

This work lays the foundation for a program of closely collaborative inverstigations between computational and experimental combustion scientists. Practical difficulties remain, including gathering suitable inlet profile specifications from the experiments, and extremely long simulation times which complicate the gathering of converged statistics of the quasi-steady

flow, in spite of the highly optimized solution strategy. Nevertheless, the resulting simulations can be used to explore experimental diagnostic assumptions and to gather higher-dimensional statistics and correlations that are simply unavailable from the experiment.

Future work will involve the incorporation of emission chemistry and further characterization of the burner configurations under a variety of fuels relevant to ultra-low emission burner scenarios. Related studies currently underway are related to turbulence/chemistry interactions across a much more broad range of fluctuation intensities, and in high-pressure environments. The studies provide valuable insight that will enable the development of reduced models for turbulent flame propagation.

References
[1] Chan C K, Lau K S, Chin W K and Chang R K 1992 *Proc. Combust. Inst.* **24** 511–518
[2] Peterson P, Olofsson J, Brackman C, Seyfried H, Zetterberg J, Richter M, Alden M, Linne M, Cheng R, Nauert A, Geyer D and Dreizler A 2007 *Appl. Opt* **46** 3928–3936
[3] Cheng R K 1991 *Combust. Flame* **101** 1–14
[4] Nogenmyr K, Peterson P, Bai X S, Nauert A, Olofsson J, Brackman C, Seyfried H, Zetterberg J, Li Z S, Richter M, Dreizler A, M, Linne and Alden M 2007 *Proc. Combust. Inst* **31** 1467–1475
[5] Mansour M and Chen Y C 2007 *Experimental Thermal Fluid Sci. in press*
[6] Cheng R K, Littlejohn D, Strakey P A and Sidwell T 2009 *Proc. Combust. Inst.* **32** 21–46
[7] Cheng R K and Littlejohn D 2008 Effects of combustion geometry on the flowfields and flame properties of a low-swirl burner *Proceedings of GT2008: ASME Turbo Expo 2008* (Berlin, Germany: ASME) paper GT2008-50504
[8] Bell J B, Cheng R K, Day M S and Shepherd I G 2007 *Proc. Combust. Inst.* **31** 1309–1317
[9] Day M S, Bell J B, Bremer P T, Pascucci V and Beckner V E 2009 *Combustion and Flame* **156** 1035–1045
[10] Rehm R G and Baum H R 1978 *N. B. S. J. Res.* **83** 297–308
[11] Ern A and Giovangigli V 1994 *Multicomponent Transport Algorithms* (*Lecture Notes in Physics* vol m24) (Berlin: Springer-Verlag)
[12] Ern A and Giovangigli V 2005 *J. Comput. Phys.* **120** 105–116
[13] Day M S and Bell J B 2000 *Combust. Theory Modelling* **4** 535–556
[14] Rendleman C A, Beckner V E, Lijewski M, Crutchfield W Y and Bell J B 2000 *Computing and Visualization in Science* **3** 147–157
[15] Nogenmyr K J, Fureby C, Bai X, Petersson P, Collin R and Linne M 2008 *Combustion Flame* **155** 357
[16] Nogenmyr K J, Fureby C, Bai X S, Petersson P, Collin R and Linne M 2009 *Combustion and Flame* **156** 25–36
[17] Yamamoto K, Ozeki M, Hayashi N and Yamashita H 2009 *Proc. Combust. Inst.* **32** 1227–1235
[18] Bell J B, Day M S, Grcar J F, Bessler W G, Schultz C, Glarborg P and Jensen A D 2002 *Proc. Combust. Inst.* **29** 2195–2202
[19] Connelly B C, Bennett B A V, Smooke M D and Long M B 2009 *Proc. Combust. Inst.* **32** 879–886